

# The impact of free electron degeneracy on collisional rates in plasmas

Gareth O. Williams,<sup>1,\*</sup> H.-K. Chung,<sup>2</sup> S. Künzel,<sup>1</sup> V. Hilbert,<sup>3</sup> U. Zastra,<sup>4</sup> H. Scott,<sup>5</sup> S. Daboussi,<sup>6</sup> B. Iwan,<sup>7</sup> A. I. Gonzalez,<sup>7</sup> W. Boutu,<sup>7</sup> H. J. Lee,<sup>8</sup> B. Nagler,<sup>8</sup> E. Granados,<sup>8</sup> E. Galtier,<sup>8</sup> P. Heimann,<sup>8</sup> B. Barbrel,<sup>9</sup> R. W. Lee,<sup>5</sup> B. I. Cho,<sup>2</sup> P. Renaudin,<sup>10</sup> H. Merdji,<sup>7</sup> Ph. Zeitoun,<sup>6</sup> and M. Fajardo<sup>1</sup>

<sup>1</sup>*GoLP/Instituto de Plasmas e Fusão Nuclear-Laboratório Associado,*

*Instituto Superior Técnico, Universidade de Lisboa, 1049-001 Lisboa, Portugal*

<sup>2</sup>*Department of Physics and Photon Science, Gwangju Institute of Science and Technology, Gwangju 61005, Korea*

<sup>3</sup>*Institute of Applied Physics, Friedrich Schiller University Jena, Albert-Einstein-Str. 6, 07745 Jena, Germany*

<sup>4</sup>*European XFEL, Holzkoppel 4, 22869 Schenefeld, Germany*

<sup>5</sup>*Lawrence Livermore National Laboratory, CA 94550, USA*

<sup>6</sup>*Laboratoire d'Optique Appliquée, ENSTA ParisTech-CNRS-École Polytechnique, UMR 7639, Chemin de la Hunière, 91762 Palaiseau, France*

<sup>7</sup>*LIDYL, CEA, CNRS and, Université Paris-Saclay, CEA Saclay 91191 Gif-sur-Yvette, France*

<sup>8</sup>*SLAC National Accelerator Laboratory, 2575 Sand Hill Road, Menlo Park, California 94025, USA*

<sup>9</sup>*Lawrence Berkeley National Laboratory, 1 Cyclotron Road, California 94720, USA*

<sup>10</sup>*CEA-DAM-DIF, Bruyères Le Châtel, 91297 Arpajon Cedex, France*

(Dated: February 20, 2019)

Degenerate plasmas, in which quantum effects dictate the behaviour of free electrons, are ubiquitous on earth and throughout space. Transitions between bound and free electron states determine basic plasma properties, yet degeneracy effects on these transitions have only been theorised. Here, we use an x-ray free electron laser to create and characterise a degenerate plasma. We show that degeneracy acts to restrict the available energy states, thereby slowing the rate of bound transitions. We couple degeneracy and bound electron dynamics in an existing collisional-radiative code, which agrees well with observations.

Many properties of dense plasmas, such as the degree of ionisation, stopping powers, and the transport of energy are shaped by electron transitions involving the free electron continuum. These transitions not only define the basic plasma properties such as the level of ionisation, but the light emitted from these transitions (the emission spectrum) is arguably the most widely used plasma diagnostic. Knowledge of the rates of these transitions is paramount in predicting the behaviour and correctly interpreting emission spectra of high-energy-density (HED) matter found throughout the universe and in HED laboratories worldwide.

In classical plasmas, the number of free electron states in the continuum is unbounded and thermal free electrons obey Maxwell-Boltzmann (MB) statistics. This description allows for a straightforward inclusion of free electrons in a multitude of theoretical treatments, including ionisation and recombination. However, this assumption is not valid in plasmas where the free electrons are governed by quantum effects (degeneracy). Quantum mechanics limits the available electron states at a given energy level through the exclusion principle, resulting in the thermal free electrons obeying Fermi-Dirac (FD) statistics. A consequence of the exclusion principle is that fully occupied states cannot accept additional electrons (Pauli blocking). Therefore, degeneracy influences electron transitions to or from the continuum by both shaping the free-electron distribution and blocking transitions to occupied states.

This simple description of the free electrons by FD statistics holds true for an idealised, homogenous system

and remains useful for understanding phenomena in more complex systems, including plasmas composed of low-Z elements. However, this picture can diverge strongly for dense plasmas of high-Z elements with more complex electronic structures. Arguably the most successful treatment of quantum effects for the free electrons of arbitrary elements is density functional theory (DFT) [1]. DFT has traditionally been applied to ground-state condensed matter systems, yet in recent years it has been used for the treatment of HED plasmas, highlighting the overlap between the condensed matter and degenerate plasma phase [2–4]. These phases co-exist in myriad HED scenarios, such as collapsing stars [5, 6], the compression phase of inertial confinement fusion (ICF) plasmas [7], shock compressed plasmas [4], the centres of large planets [8] and the early stages of all high intensity optical or x-ray laser interactions with solids [9, 10]. Furthermore, degenerate plasmas can exist at any temperature, provided the electron density is sufficiently high.

However, the explicit calculation of processes involving bound and free electrons plus photons for a multitude of electronic levels required for many HED and astrophysical applications is not tractable within the framework of DFT. Collisional-radiative (CR) codes [12], initially designed for hot, low-density plasmas, are the tools of choice for these situations. However, CR codes usually do not treat degeneracy of the free electrons. A tractable method for including free-electron quantum effects in these codes is pivotal in bridging the gap between the often co-existing condensed matter and plasma phases.

In this Letter, we present x-ray fluorescence spectro-

scopic measurements of a degenerate solid-density aluminium plasma to elucidate free electron degeneracy effects on atomic transitions. The measured fluorescence spectra show marked differences to those predicted by models using a classical MB treatment of the free electrons. We show that by correcting the rates of atomic processes in a CR code using FD statistics to account for degeneracy, a good match with the data be found, but only when using a differential cross-section peaked at low energy. The effects of degeneracy accentuate the effects of different cross-section profiles, making them experimentally distinguishable.

Theoretical treatments predict a substantial (several orders of magnitude) reduction of the rates of collisional ionisation and recombination with increasing degeneracy, yet experimental confirmation is so far lacking [11–13]. To test these predictions, the rate of collisional ionisation or recombination must be measured in a plasma of known degeneracy. Experimentally, this presents a significant challenge: first, collisional ionisation of solids requires temperatures well above those in the degenerate regime at solid density, making a transient non-equilibrium measurement necessary, and second, the level of degeneracy (electron temperature and density) must be well defined during the measurement.

The intensities and pulse durations now available at x-ray free electron laser (XFEL) facilities have naturally led to the creation of plasma states with well defined temperatures and densities from solid targets [14, 15]. Uniquely, the ultrashort nature of XFEL pulses (typically <100 fs) and tuneable photon energy allow the x-ray fluorescence signature of the plasma to be measured before significant changes in the ion density occur (due to target expansion) [16]. Similar techniques have facilitated the measurement of ionisation potential depression [3, 17, 18], collisional rates [19, 20], saturable [21, 22] and reverse-saturable [23] x-ray absorption, and x-ray opacities of solid density plasmas [24]. The XFEL pulse can be tailored to create a small population of high energy electrons to drive ionisation in an otherwise degenerate plasma background, while simultaneously providing the XFEL induced fluorescence spectrum characteristic of the level of ionisation, making it an ideal tool for investigating degenerate plasmas.

We use the Linear Coherent Light Source (LCLS) XFEL [25] and the Matter in Extreme Conditions instrument [26] to deliver pulses of 37  $\mu\text{J}$  in energy, 35 fs in duration at full-width-at-half-maximum, with a photon energy of 3 keV, to heat solid foils of aluminium of 300 and 600 nm in thickness. The XFEL beam is focussed with a stack of beryllium lenses to a spot of about 25  $\mu\text{m}$  in diameter. The pathway of XFEL-induced fluorescent emission starts with the absorption of an incoming photon of  $E^{XF} = 3 \text{ keV}$ , exciting a  $K$ -shell electron at a binding energy of  $E^K \approx 1560 \text{ eV}$  to an energy of  $E^{XF} - E^K \approx 1440 \text{ eV}$  (where  $K$ ,  $L$  and  $M$  correspond to

the first, second and third electrons shells, respectively). The subsequent filling of the  $K$ -shell hole occurs via an  $L$ -shell electron relaxing to the vacant  $K$ -shell hole. In aluminium, this  $L$  to  $K$  shell transition releases an energy of  $E^{LK} \approx 1485 \text{ eV}$  and results in the emission of an Auger electron at an energy of  $E^A \approx E^{LK} - E^L \approx 1400 \text{ eV}$ , where  $E^L$  is the binding energy of the  $L$ -shell electron. Auger emission accounts for about 96% of the recombination events, leaving two holes in the  $L$ -shell. The other 4% of recombination events relax via the emission of a photon, and these photons constitute the measured fluorescence spectrum.

The fluorescence of the photo-ionised solid density plasma was recorded using an x-ray spectrometer with a 001 orientation Rubidium Hydrogen Phthalate (RAP) crystal of 100  $\mu\text{m}$  thickness places on substrate a 5 cm radius of curvature that focussed the fluorescent emission onto an x-ray detector. An aluminium filter of 1.6  $\mu\text{m}$  thickness was used at the spectrometer entrance to reject optical light. The spectral resolution of the system was  $\sim 1 \text{ eV}$ . More than 100 shots were accumulated for each measurement. To infer the plasma conditions, the XFEL spot profile was measured using imprints of the ablation pattern for a range of fluence values (F-scan) as shown in Fig.1a [27, 28]. This measurement, when combined with an XUV emission spectrum measurement shown in [2], allowed us to confirm a peak electron temperature of  $\sim 12 \text{ eV}$  in the hottest, central region of the plasma ( $R1$  in Fig.1a). Since the total pulse energy is spread over a much larger region, we divide the plasma into ten concentric volumes, each of which absorb the same number of XFEL photons (we select regions  $R1$ ,  $R4$ ,  $R7$  and  $R10$  for clarity, shown in Fig.1a).

The absorption of XFEL photons results in a population of high energy photoionised and Auger electrons with energies of  $\sim 1.4 \text{ keV}$ , that will be referred to as hot electrons. The electrons that constitute the cold-solid free electrons remain thermalized, and will be referred to as the bulk electrons. To estimate the degeneracy of the bulk electrons, as characterized by  $\Theta = \mu/k_B T_e$ , where  $\mu$  is the chemical potential of the plasma and  $T_e$  the bulk electron temperature, we must model the temperature as a function of time. The bulk electrons (and hence the degeneracy) are initially unaffected by the XFEL photons, and heat up only after a time delay relative to the XFEL pulse. We define this delay as the difference in time between the XFEL pulse and bulk electron heating, meaning a time delay of zero would correspond to instant thermalisation of the XFEL energy into the bulk electrons. We have used delay times in our calculations which approximately agree with recently reported thermalisation times of XFEL generated hot electrons in silicon [29].

The time evolution of the bulk electron temperature within a selection of the volumes labelled  $R$  are shown in Fig.1b for two separate time delays, 20 fs and 40 fs. De-

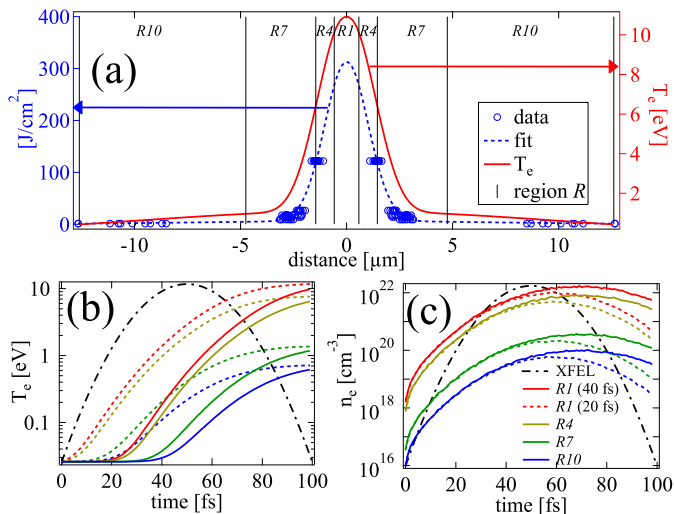


FIG. 1. The fluence scan data (blue circles) with fitted curve (dashed blue line) and corresponding peak electron temperatures (solid red line) of the XFEL focal spot radial profile (a). The spot is separated into ten radial volumes for modelling, labelled  $R$ , that absorb the same number of XFEL photons, and four such regions are shown vertical by black lines in (a). The XFEL pulse intensity profile in time (black dash-dot curve) and corresponding electron temperatures for two heating delays of 20 fs (dashed curves) and 40 fs (solid curves) for four plasma volumes (b). The corresponding hot electron density,  $n_e$ , are shown in (c).

tails of the bulk electron temperature calculations are reported elsewhere [2, 30]. The corresponding hot electron density is shown as function of time in Fig. 1c. Modelling of the bulk electron temperature shows that the plasma remains degenerate throughout the XFEL pulse (as  $T_e < E_F$ , where  $E_F \approx 12$  eV is the Fermi energy of aluminium at room temperature). The XFEL radiation, bulk electron temperatures and hot electron densities in Figs. 1b and 1c are used as input into a CR code to model the fluorescence spectrum, as discussed later.

The bulk electrons never reach a temperature sufficient to cause appreciable ionisation of the  $L$ -shell. On the other hand, the hot electrons can repeatedly collisionally ionise the  $L$ -shell until their energy is below that of the ionisation threshold. Ultimately, the energy of the hot electrons is transferred to the bulk electrons, leading to increased  $T_e$  (see Figs. 1b and 1c). Ionisation of the  $L$ -shell by the hot electrons causes a reduction in screening and increased  $K$ -shell binding energy, resulting in  $K\alpha$  fluorescence at higher photon energies. These photons are referred to  $K\alpha$  satellites, and are directly related to the number of vacancies in the  $L$ -shell at the time of photon emission, irrespective of the exact electron configuration in the  $L$ -shell. For the satellites to be observed in the measured spectrum, holes in the  $L$ -shell must be present at the time the fluorescent  $L$  to  $K$  transition takes place.

In this way, the fluorescent emission spectrum reflects the  $L$ -shell vacancies present only within the temporal envelope XFEL pulse.

To quantify the degeneracy effect on atomic rates, a correction factor,  $CF$ , is defined as the ratio of the atomic rate including degeneracy,  $A^{FD}$ , to that without degeneracy,  $A^{MB}$ , ( $CF = \frac{A^{FD}}{A^{MB}}$ ). The  $CF$  values are calculated following theoretical frameworks presented elsewhere, and are plotted as a function of degeneracy,  $\Theta$ , in Fig. 2 (see caption for details) [11–13]. The two processes dominating the number of  $L$ -shell vacancies in time are collisional ionisation (CI) and its inverse process, three-body recombination (3BR), which are shown as dashed and solid curves in Fig. 2, respectively. The range of  $CF$  values corresponding to the plasma conditions at the peak of fluorescent emission for charge states V and VI ( $\sim 60$  fs) for heating delays of 20 fs and 40 fs are indicated in Fig. 2 by dash-dot lines with arrows.

Calculating the rate,  $A$ , of a collisional process requires integrating the product of the electron distribution,  $f_e(E)$ , and the cross-section,  $\sigma(E)$ , for that process ( $A \propto \int \sigma(E)f_e(E)dE$ ) over electron energy  $E$ . As the rates depend on the choice of the cross-section,  $\sigma(E)$ , we explore the effect of several cross-section models on the values of  $CF$  for comparison. The correction factor can then applied straightforwardly to the classical MB rate as  $CF \times A^{MB}$ , for a given level of degeneracy,  $\Theta$ .

First we calculate  $CF$  for several collisional ionization cross-sections commonly used in CR codes, namely BC [31], BCF [20] and Lotz [32] which are shown as the shaded green curve for 3BR and dashed green for CI curves in Fig. 2. These expressions give values for total cross-sections as a function of energy  $E$  of the ionizing electron. Calculating  $CF$  for a degenerate electron distribution requires knowing the differential cross-section as a function of both (outgoing) electron energies, as separate blocking factors apply to these electrons. However, models or experiments of such differential cross sections for degenerate plasmas are absent. The green curves in Fig. 2 assume the differential cross-section for each value of  $E$  is flat, i.e. independent of the energy of the outgoing electrons. These three cross-sections then yield similar values of  $CF$ . A simplified total cross-section with a  $1/E$  dependance provides a good approximation while simplifying the calculation of  $CF$  considerably. We refer to this as the analytical cross-section, and the corresponding values of  $CF$  are shown in red in Fig. 2. Using the analytical cross-section results in values of  $CF$  roughly an order of magnitude lower than the BC, BCF and Lotz values. This is due to the strong weighting of the analytical cross-section ( $1/E$ ) on lower electron energies, where the differences between the FD and MB distributions at low temperatures are maximised and where blocking factors become important.

In the present study, the collisional ionisation is driven by the hot electrons that have energies orders of magni-

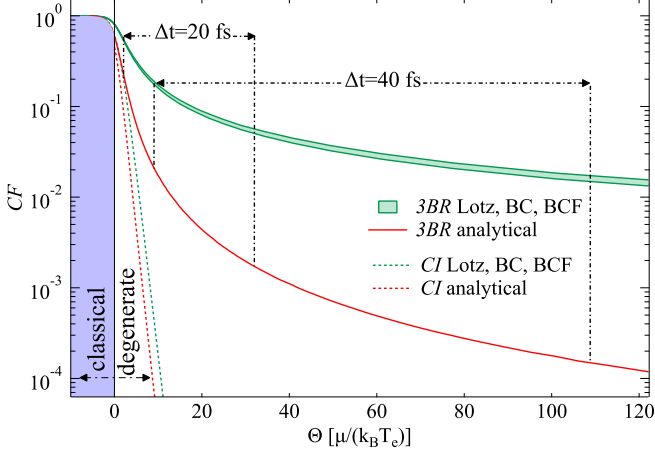


FIG. 2. The correction factor for the collisional rates,  $CF$ , plotted against the plasma degeneracy  $\Theta = \mu/k_B T_e$ , from the classical to the degenerate regime, for an electron density of  $1.8 \times 10^{23} \text{ cm}^{-3}$  and varying bulk electron temperature  $T_e$ . Values of  $CF$  are shown for three-body-recombination (3BR) (green shaded curve) and collisional ionisation (CI) (dashed green curve) for three commonly used cross sections for an electron transition of energy  $dE \gg T_e$  (details in text).  $CF$  values for the analytical cross sections are shown for three-body-recombination (solid red curve) and ionisation (dashed red curve). The range of values for  $CF$  for the two heating delays used in this model are marked (black dash-dot lines with arrows).

tude greater than the Fermi energy. After the collision, the ionised and scattered electrons are therefore born at energies for which Pauli blocking is negligible. Conversely, three-body recombination occurs through the degenerate bulk electrons relaxing to vacant bound states. Therefore, the degeneracy correction to the collisional ionisation by hot electrons is negligible ( $CF = 1$ ) and we can isolate the dominant process affected by degeneracy as three-body recombination. Contrary to collisional ionisation cross-sections, models or measurements of three-body recombination cross-sections are greatly lacking and its shape is not accurately known. Consequently, the three-body recombination cross-section must be approximated from the collisional-ionisation cross-section through the principle of detailed balance [33].

Two XFEL induced  $K$ -shell fluorescent spectra for target thicknesses of 300 nm and 600 nm are shown in Fig. 3 (black solid and dashed lines). A negligible difference between the normalised spectra of both thicknesses is found, showing that the plasma is optically thin for the range of photon energies shown in Fig. 3. The three peaks **IV**, **V** and **VI** visible in Fig. 3 correspond to the fluorescent ( $L$  to  $K$ ) transitions with one, two and three  $L$ -shell vacancies, respectively. Qualitatively, the appearance of satellites in the spectra signify that there are  $L$ -shell holes present at the time of fluorescence, which occurs during the XFEL pulse.

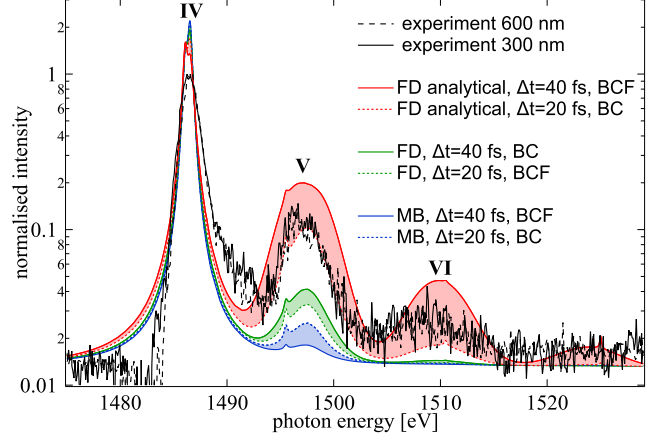


FIG. 3. The experimental  $K\alpha$  fluorescence spectrum of XFEL irradiated aluminium showing the three ionisation stages **IV**, **V** and **VI** for 300 nm and 600 nm foil thickness (dashed black and solid black line, respectively). Each shaded region is calculated using a different treatment of  $CF$  according to Fig. 2. The spectra of two heating delays, and three cross-sections are calculated for each treatment of  $CF$ . The spectra using MB statistics and no correction (shaded blue region), FD statistics with the standard  $CF$  values (shaded green region), and FD statistics with the analytical approximation (shaded red region) are shown.

To quantitatively compare our measured spectrum with theoretical predictions, we use the time-dependant non-local-thermodynamic-equilibrium (non-LTE) CR code SCFLY [34–36], which includes effects of both degenerate and non-thermal electron distributions. SCFLY has shown to be a robust tool for the analysis of similar experiments, albeit at higher temperatures [3, 16, 17, 19, 20, 22–24].

Evolving a non-thermal free electron distribution that is fully self-consistent with all of the atomic processes is beyond the scope of this Letter. Instead, we approximate the shape of the hot electron distribution in time to be in broad agreement with other studies [37, 38], and define a hot electron density that conserves the energy balance between the XFEL pulse, bulk, and hot electrons. The non-thermal distribution is shaped to capture the main features of the hot electron energy distribution, and consists of a peak at  $\sim 1410$  eV representing the photo and Auger electrons from the XFEL pulse, and a smaller ( $\sim 10\%$  of the main photo-peak) peak at 2.9 keV that represents the  $L$ -shell electrons photoionised by the XFEL pulse. The electrons born at these energies then relax by losing their energy in  $\sim 70$  eV steps due to collisional ionisation of the  $L$ -shell. We note that the  $K\alpha$  emission spectrum is insensitive to the exact shape of the hot electron distribution. As the total change in electron density is minimal, the spectra are insensitive to the ionisation potential depression model used [3, 17, 18]. The bulk electron temperature (Fig. 1b), hot electron density

(Fig.1c) and distribution are input into SCFLY for every time-step.

Spectra calculated using SCFLY with MB and FD statistics and different cross-section models are shown in Fig. 3 (shaded curves). The spectra using classical MB statistics in Fig. 3 (blue shaded curve) show a cold **IV** peak, and a negligible **V** peak that do not agree well with the experimentally observed spectra. A standard interpretation of the ratio of the satellite intensities suggests a plasma with an average electron temperature of  $T_e \approx 20$  eV. This disagrees sharply with the average  $T_e$  of a few eV's from energy deposition measurements in Fig.1, and a peak  $T_e \approx 13$  eV obtained from soft x-ray emission spectra [2]. Having tested a range of time delays and cross-sections, we could not obtain good agreement with the data when using MB statistics. As the spectra of hot aluminium plasmas have been shown elsewhere [16] to be well reproduced by SCFLY in the classical regime, the discrepancy between the experimental data and spectra calculated assuming classical statistics here shows that reconsidering the rates in the degenerate regime is essential.

Adding the correction factors for the common cross sections (BC, BCF and Lotz) to the collisional rates in SCFLY produces more prominent satellites and a much improved fit to the data (Fig. 3 shaded green curve). Although a good match to the data is still lacking with these corrections, the main effect of decreased three-body recombination rates is evident from the increased prominence of the  $K\alpha$  satellites. As the three-body recombination rate is suppressed, the  $L$ -shell holes persist longer than they would in the absence of degeneracy, causing more prominent satellite peaks. Since these cross-sections have performed well in classical plasmas, we then apply the values of  $CF$  calculated using the analytical approximation to these rates in SCFLY. This yields a good fit to the data, in which the difference between spectra calculated using the cross-sections and delay times lie within the error of experimental data. Although the  $1/E$  shape of the analytical cross-section is an approximation, these results strongly suggest that correction factors for three-body recombination are better approximated with cross sections favouring lower electron energies.

In conclusion, we have used the simultaneous pump-and-probe method [16] to create and diagnose a degenerate solid density aluminium plasma with an XFEL. We have shown that the resulting fluorescence spectrum is not reproduced with standard treatments that assume a classical MB free-electron distribution. By adding degeneracy corrections,  $CF$ , to the collisional rates in SCFLY, we demonstrated a good fit to the data when using cross-sections peaked at low electron energy. We identified the driving factor that causes differences between the calculated MB and FD spectra to be the lowered three-body recombination rate in this study. This work has shown experimentally that degenerate plasmas exhibit

behaviour that differs significantly from classical predictions. The method of using correction factors to the rates is applicable to any collisional-radiative code. The results here will lead to a more accurate understanding and greater control of a wide variety of degenerate and non-equilibrium HED states.

Use of the Linac Coherent Light Source (LCLS), SLAC National Accelerator Laboratory, is supported by the U.S. Department of Energy, Office of Science, Office of Basic Energy Sciences under Contract No. DE-AC02-76SF00515. The MEC instrument is supported by the U.S. Department of Energy, Office of Science, Office of Fusion Energy Sciences under contract No. SF00515. We acknowledge support from Fundação para a Ciência e a Tecnologia (FCT) projects EXPL/FIS-OPT/0889/2012, PTDC/FIS/112392/2009 and 02/SAICT/2017/31868, COST Action CA17126, Laserlab-Europe EU-H2020 654148, and Swedish Foundation for International Cooperation in Research and Higher Education (STINT). This work was supported by the European Unions Horizon 2020 research and innovation programme (VOXEL H2020-FETOPEN-2014-2015-RIA 665207). H.-K.C. and B.I.C. acknowledge support for the National Research Foundation (NRF-2015R1A5A1009962 and NRF-2016R1A2B4009631) of Korea. The work of H. Scott was performed under the auspices of the U.S. Department of Energy by Lawrence Livermore National Laboratory under Contract DE-AC52-07NA27344.

---

\* gareth.williams@ist.utl.pt

- [1] E. K. Gross and R. M. Dreizler, *Density functional theory*, Vol. 337 (Springer Science & Business Media, 2013).
- [2] G. O. Williams, S. Künzel, S. Daboussi, B. Iwan, A. Gonzalez, W. Boutu, V. Hilbert, U. Zastrau, H. Lee, B. Nagler, *et al.*, *Physical Review A* **97**, 023414 (2018).
- [3] S. Vinko, O. Ciricosta, and J. Wark, *Nature communications* **5** (2014).
- [4] L. Fletcher, H. Lee, T. Döppner, E. Galtier, B. Nagler, P. Heimann, C. Fortmann, S. LePape, T. Ma, M. Millot, *et al.*, *Nature Photonics* **9**, 274 (2015).
- [5] H. Van Horn, *Science* **252**, 384 (1991).
- [6] G. Chabrier, F. Douchin, and A. Potekhin, *Journal of Physics: Condensed Matter* **14**, 9133 (2002).
- [7] J. Lindl, *Physics of plasmas* **2**, 3933 (1995).
- [8] F. Coppari, R. Smith, J. Eggert, J. Wang, J. Rygg, A. Lazicki, J. Hawreliak, G. Collins, and T. Duffy, *Nature Geoscience* **6** (2013).
- [9] S. P. Hau-Riege, *High-Intensity X-rays-Interaction with Matter: Processes in Plasmas, Clusters, Molecules and Solids* (John Wiley & Sons, 2012).
- [10] P. Gibbon, *Short Pulse Laser Interactions with Matter: An Introduction* (Imperial College Press, 2005).
- [11] G. Tallents, *High Energy Density Physics* **20**, 9 (2016).
- [12] Y. Ralchenko, *Modern methods in collisional-radiative modeling of plasmas*, Vol. 90 (Springer, 2016).
- [13] G. Tallents, *An introduction to the atomic and radiation*

- physics of plasmas* (Cambridge University Press, 2018).
- [14] R. Lee, S. Moon, H.-K. Chung, W. Rozmus, H. Baldis, G. Gregori, R. Cauble, O. Landen, J. Wark, A. Ng, S. Rose, C. Lewis, D. Riley, J.-C. Gauthier, and P. Audebert, *J. Opt. Soc. Am. B* **20**, 770 (2003).
  - [15] A. Levy, P. Audebert, R. Shepherd, J. Dunn, M. Cammarata, O. Ciricosta, F. Deneuille, F. Dorchies, M. Fajardo, C. Fourment, *et al.*, *Physics of Plasmas* (1994-present) **22**, 030703 (2015).
  - [16] S. Vinko, O. Ciricosta, B. Cho, K. Engelhorn, H.-K. Chung, C. Brown, T. Burian, J. Chalupský, R. Falcone, C. Graves, *et al.*, *Nature* **482**, 59 (2012).
  - [17] O. Ciricosta, S. M. Vinko, H.-K. Chung, B. I. Cho, C. R. D. Brown, T. Burian, J. Chalupský, K. Engelhorn, R. W. Falcone, C. Graves, V. Hájková, A. Higginbotham, L. Juha, J. Krzywinski, H. J. Lee, M. Messerschmidt, C. D. Murphy, Y. Ping, D. S. Rackstraw, A. Scherz, W. Schlotter, S. Toleikis, J. J. Turner, L. Vysin, T. Wang, B. Wu, U. Zastra, D. Zhu, R. W. Lee, P. Heimann, B. Nagler, and J. S. Wark, *Phys. Rev. Lett.* **109**, 065002 (2012).
  - [18] O. Ciricosta, S. Vinko, B. Barbrel, D. Rackstraw, T. Preston, T. Burian, J. Chalupský, B. I. Cho, H.-K. Chung, G. Dakovski, *et al.*, *Nature communications* **7**, 11713 (2016).
  - [19] S. Vinko, O. Ciricosta, T. Preston, D. Rackstraw, C. Brown, T. Burian, J. Chalupský, B. Cho, H.-K. Chung, K. Engelhorn, *et al.*, *Nature communications* **6** (2015).
  - [20] Q. Y. van den Berg, E. V. Fernandez-Tello, T. Burian, J. Chalupský, H.-K. Chung, O. Ciricosta, G. L. Dakovski, V. Hájková, P. Hollebon, L. Juha, J. Krzywinski, R. W. Lee, M. P. Minitti, T. R. Preston, A. G. de la Varga, V. Vozda, U. Zastra, J. S. Wark, P. Velarde, and S. M. Vinko, *Phys. Rev. Lett.* **120**, 055002 (2018).
  - [21] H. Yoneda, Y. Inubushi, M. Yabashi, T. Katayama, T. Ishikawa, H. Ohashi, H. Yumoto, K. Yamauchi, H. Mimura, and H. Kitamura, *Nature communications* **5**, 5080 (2014).
  - [22] D. Rackstraw, O. Ciricosta, S. Vinko, B. Barbrel, T. Burian, J. Chalupský, B. Cho, H.-K. Chung, G. Dakovski, K. Engelhorn, *et al.*, *Physical review letters* **114**, 015003 (2015).
  - [23] B. I. Cho, M. S. Cho, M. Kim, H.-K. Chung, B. Barbrel, K. Engelhorn, T. Burian, J. Chalupský, O. Ciricosta, G. L. Dakovski, V. Hájková, M. Holmes, L. Juha, J. Krzywinski, R. W. Lee, C. H. Nam, D. S. Rackstraw, S. Toleikis, J. J. Turner, S. M. Vinko, J. S. Wark, U. Zastra, and P. A. Heimann, *Phys. Rev. Lett.* **119**, 075002 (2017).
  - [24] T. R. Preston, S. M. Vinko, O. Ciricosta, P. Hollebon, H.-K. Chung, G. L. Dakovski, J. Krzywinski, M. Minitti, T. Burian, J. Chalupský, V. Hájková, L. Juha, V. Vozda, U. Zastra, R. W. Lee, and J. S. Wark, *Phys. Rev. Lett.* **119**, 085001 (2017).
  - [25] P. Emma, R. Akre, J. Arthur, R. Bionta, C. Bostedt, J. Bozek, A. Brachmann, P. Bucksbaum, R. Coffee, F. Decker, Y. Ding, D. Dowell, S. Edstrom, A. Fisher, J. Frisch, S. Gilevich, J. Hastings, G. Hays, P. Hering, Z. Huang, R. Iverson, H. Loos, M. Messerschmidt, A. Miahnahri, S. Moeller, H.-D. Nuhn, G. Pile, D. Ratner, J. Rzeplia, D. Schultz, T. Smith, P. Stefan, H. Tompkins, J. Turner, J. Welch, W. White, J. Wu, Y. G., and G. J., *Nat. Photonics* (2010).
  - [26] B. Nagler, B. Arnold, G. Bouchard, R. F. Boyce, R. M. Boyce, A. Callen, M. Campell, R. Curiel, E. Galtier, J. Garofoli, E. Granados, J. Hastings, G. Hays, P. Heimann, R. W. Lee, D. Milathianaki, L. Plummer, A. Schropp, A. Wallace, M. Welch, W. White, Z. Xing, J. Yin, J. Young, U. Zastra, and H. J. Lee, *Journal of Synchrotron Radiation* **22**, 520 (2015).
  - [27] J. Chalupský, J. Krzywinski, L. Juha, V. Hájková, J. Cihelka, T. Burian, L. Vyšín, J. Gaudin, A. Gleason, M. Jurek, A. R. Khorsand, D. Klinger, H. Wabnitz, R. Sobierajski, M. Störmer, K. Tiedtke, and S. Toleikis, *Opt. Express* **18**, 27836 (2010).
  - [28] P. Heimann, M. MacDonald, B. Nagler, H. J. Lee, E. Galtier, B. Arnold, and Z. Xing, *Journal of synchrotron radiation* **23** (2016).
  - [29] T. Pardini, J. Alameda, A. Aquila, S. Boutet, T. Decker, A. E. Gleason, S. Guillet, P. Hamilton, M. Hayes, R. Hill, J. Koglin, B. Kozioziemski, J. Robinson, K. Sokolowski-Tinten, R. Soufli, and S. P. Hau-Riege, *Phys. Rev. Lett.* **120**, 265701 (2018).
  - [30] G. Williams, H.-K. Chung, S. Vinko, S. Künzel, A. Sardinha, P. Zeitoun, and M. Fajardo, *Phys. Plasmas* **20**, 042701 (2013).
  - [31] A. Burgess and M. C. Chidichimo, *Monthly Notices of the Royal Astronomical Society* **203**, 1269 (1983).
  - [32] W. Lotz, *Zeitschrift für Physik A Hadrons and Nuclei* **216**, 241 (1968).
  - [33] J. Oxenius, *Kinetic theory of particles and photons: theoretical foundations of non-LTE plasma spectroscopy*, Vol. 20 (Springer Science & Business Media, 2012).
  - [34] H.-K. Chung, M. H. Chen, W. L. Morgan, Y. Ralchenko, and R. W. Lee, *High Energy Density Phys.* **1**, 3 (2005).
  - [35] R. W. Lee and J. T. Larsen, *Journal of Quantitative Spectroscopy and Radiative Transfer* **56**, 535 (1996).
  - [36] H.-K. Chung, W. Morgan, and R. Lee, *Journal of Quantitative Spectroscopy and Radiative Transfer* **81**, 107 (2003), radiative Properties of Hot Dense Matter.
  - [37] A. G. de la Varga, P. Velarde, F. de Gaufridy, D. Portillo, M. Cotel, A. Barbas, A. González, and P. Zeitoun, *High Energy Density Physics* **9**, 542 (2013).
  - [38] R. Royle, Y. Sentoku, R. C. Mancini, I. Paraschiv, and T. Johzaki, *Physical Review E* **95**, 063203 (2017).